Ultrasound-modulated optical imaging using a confocal Fabry-Perot interferometer and a powerful long pulse laser

Rousseau, Guy; Blouin, Alain; Monchalin, Jean-Pierre

Publisher's version / Version de l'éditeur:
https://doi.org/10.1117/12.807960
Photons Plus Ultrasound: Imaging and Sensing 2009, pp. 71771E-1-71771E-9, 2009-02

Ultrasound-modulated optical imaging using a confocal Fabry-Perot interferometer and a powerful long pulse laser

Guy Rousseau,* Alain Blouin and Jean-Pierre Monchalin
Industrial Materials Institute, National Research Council Canada,
75 de Mortagne Blvd., Boucherville, Québec, Canada, J4B 6Y4

ABSTRACT

Ultrasound-modulated optical imaging combines the good spatial resolution of ultrasonic waves (mm scale) and the spectroscopic properties of light to detect optically absorbing objects inside thick (cm scale) highly scattering media. Light propagating in a scattering medium can interact with an ultrasonic wave thereby being tagged by a frequency shift equal to the ultrasound frequency or its harmonics. In this paper, a confocal Fabry-Perot interferometer (CFPI) is used as a tunable spectral filter to detect selectively the ultrasound-tagged photons. The CFPI allows obtaining high spectral resolution (MHz scale) while maintaining a high light gathering power when compared to other spectroscopic devices of comparable resolution. The contrast between the tagged photons and the untagged photons can be further enhanced by cascading CFPI. Moreover, the fast response of the CFPI allows performing measurements within the speckle decorrelation time typically encountered in biomedical applications. In this paper, the use of a single-frequency laser emitting powerful optical pulses allows illuminating the scattering medium only during the transit time of the probing ultrasonic pulses. Consequently, the acoustic and the optical power are both concentrated in time to enhance the signal-to-noise ratio of the technique while remaining below the biomedical safety limits. The detection of optically absorbing objects (mm size) inside 30- and 60-mm thick scattering media is presented.

Keywords: biomedical imaging, ultrasound-modulated optical tomography, acousto-optical imaging, ultrasound-tagged photons, scattering media, confocal Fabry-Perot interferometer, pulsed single-frequency laser

1. INTRODUCTION

Optical imaging techniques for biomedical diagnostics are currently very actively developed. These techniques have the advantage of being based on non-ionizing radiation while being able to provide morphological as well as functional information [1]. Ultrasound-modulated optical imaging (or tomography) is an emerging technique which allows the localization of an optically absorbing object imbedded in an optically scattering medium through the detection of ultrasound-modulated photons [2-9]. This method combines the good spatial resolution (mm scale) and the penetration depth (cm scale) of ultrasound waves with the spectroscopic information provided by light. A practical limit of this technique is its poor sensitivity or low signal-to-noise ratio (SNR). Even though the optical absorption of water is relatively low in the therapeutic window, the strong scattering of photons propagating in tissues reduces significantly the number of collectable photons. Moreover, for biomedical applications, safety considerations limit the power level of both the ultrasonic wave and the laser beam. The peak negative pressure of the ultrasonic wave must remain below a value prescribed by the so-called mechanical index (MI) to avoid cavitation and its side effects [10]. Similarly, the laser beam irradiance must be maintained below the maximum permissible exposure (MPE) to avoid heating damage [11].

In ultrasound-modulated imaging, the tagged photons can be detected by full field imaging of the speckle pattern with an array of detectors (CCD camera) [4-5] or by interferometric schemes using a single photodetector [3,6-8]. Methods based on arrays of detectors require intensive data processing but provide a better SNR [4-5]. The interferometric scheme is either based on a confocal Fabry-Perot interferometer (CFPI) [3] or on a photorefractive interferometer (PRI) [6-8]. Both instruments present a large optical etendue when compared to other interferometers but their etendue is still much lower than the etendue of the scattered optical beam. The detection of scattered photons thus remains an inefficient process. More recently, an atomic bandpass filter based on spectral hole burning (SHB) in a cryogenically cooled crystal has been investigated [9]. This last technique provides a higher optical etendue.

* guy.rousseau@cnrc-nrc.gc.ca

In ultrasound-modulated optical imaging, most photons in the signal beam are not modulated since the insonified zone in the scattering medium is much smaller than the illuminated zone. Consequently, the number of ultrasonically tagged photons is much lower than the number of untagged photons. In this respect, methods based on the rejection of the untagged photons (CFPI and SHB) are more attractive since the detector is essentially illuminated by the useful tagged photons. Otherwise, even for quantum limited measurements, the shot noise of the numerous untagged photons will deteriorate the SNR. Even though the SHB filter is more attractive in terms of optical etendue, its use is limited to a specific wavelength determined by the atomic transition of the doping element. This may imply the development and use of multiple laser media for multi-wavelength measurements which may be essential for clinical applications. On the contrary, the CFPI is intrinsically broadband. The use of broadband multilayer dielectric coatings allows a single CFPI to be used over a continuous bandwidth in the visible or in the near infrared. In the first implementation of the CFPI-based detection scheme [3], high-frequency ultrasound waves were used to obtain an acceptable rejection of the untagged photons with a 50-cm long single-pass CFPI of moderate finesse. With a CFPI, the detection of faint spectral lines close to a strong one is limited by technically attainable values of the finesse and resonator length [12]. This difficulty can be surmounted by cascading multiple interferometers or by using a multipass configuration [13,14]. In this work, we consider the use of a double-pass configuration.

The limited optical etendue remains the main drawback of the CFPI. A direct way to enhance the number of tagged photons detected at the exit of the CFPI is to increase the optical power incident on the scattering medium. However, in order to respect the MPE in terms of average power, the increase of the instantaneous power must be counterbalanced by a reduction of the exposure duration. This suggests the use of a train of pulses of high peak power with an appropriate duty cycle. In such a situation, the number of photons is high only for the relevant period of time, that is, during the transit time of the ultrasonic toneburst in the scattering medium. For a given average optical power, the use of a low duty cycle pulse train is advantageous in terms of SNR because it becomes easier to overcome the technical noise. Ultimately, each single-shot measurement should be limited only by the shot noise of the tagged photons by properly eliminating the untagged ones.

In this paper, we describe an experiment based on the use of a high-peak-power long-pulse single-frequency laser at 1.064 μm. Photons are tagged in 30- and 60-mm thick scattering media with 10-cycles ultrasonic tonebursts generated by a 5-MHz focused transducer. The tagged photons are detected with a tunable, actively stabilized, double-pass CFPI.

2. EXPERIMENTAL SETUP

2.1 Optical setup

In our experiment, a double-pass CFPI was used as a bandpass filter for the detection of photons tagged by a frequency shift equal to the ultrasound frequency or its harmonics. The experimental setup is schematically shown in Fig. 1. The single-frequency laser pulses (1.064-μm wavelength) emitted by a Nd:YAG master oscillator power amplifier (MOPA) illuminate the cell containing the scattering medium (SM). The SM is insonified with a focused ultrasonic transducer (UT: 19-mm diameter, 45-mm focal length) fed with 10-cycle bursts at 5 MHz. At the rear face of the SM, photons are injected in a multimode collecting optical fiber (COF: 1-mm core diameter, numerical aperture: 0.36) and sent toward the double-pass CFPI. The beam exiting from the COF is collimated with a lens and polarized by a polarizing beamsplitter (PBS). The beam is then coupled in the CFPI for a first pass. The 1-m long CFPI is characterized by a free spectral range (FSR) of 75 MHz and a finesse F = 28 (mirror reflectivity: 95%). The beam exiting from the CFPI is reflected back by a plane mirror (PM). A quarter-wave plate (QW) is used to rotate the polarization of the reflected beam by 90°. The beam exiting after the second pass is redirected by the PBS toward an InGaAs-PIN photodiode (PD: 0.5-mm active diameter, 400-kHz bandwidth). The optical etendue of the CFPI (0.38 mm^2 sr) was adapted to that of the COF (0.33 mm^2 sr). In the double-pass configuration, the effective finesse was ~ 40 resulting in a spectral filter with a full-width-at-half-maximum (FWHM) of 1.8 MHz. This value was adapted to the FWHM of the toneburst power spectrum (0.5 MHz) and sufficiently narrow to separate the tagged photons from the untagged ones. The double-pass configuration allows a rejection of the untagged photons by 22 dB when the transmission peak of the CFPI is offset by 5 MHz to coincide with the first sideband of tagged photons and by 33 dB for an offset of 10 MHz.

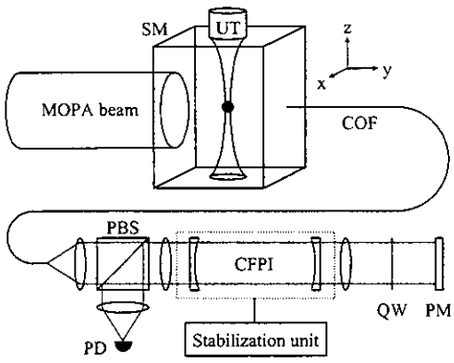

Figure 1 Schematic diagram of the setup for the ultrasound-modulated optical imaging experiment. MOPA: master oscillator power amplifier, SM: scattering medium, UT: ultrasonic transducer, COF: collecting optical fiber, PBS: polarizing beam splitter, CFPI: confocal Fabry-Perot interferometer, QW: quarter-wave plate, PM: plane mirror, PD: photodetector. The black sphere in the SM represents the typical position of the absorbing object.

The CFPI, when used as a spectral filter, is characterized by a transmission curve with non negligible wings even for a relatively high finesse. The transmission curve of a single-pass CFPI with F = 28 and FSR = 75 MHz is shown (solid line) in Fig. 2(a). The transmission curve of the same CFPI used in the double-pass configuration is simply equal to the square of the single-pass configuration. This curve (dotted line) is also shown in Fig. 2(a). It is easily seen that the width of the wings is reduced significantly. The same curves are shown in Fig. 2(b) in terms of the rejection (in dB) as a function of the frequency detuning. It is seen that the maximum rejection obtained in the single-pass configuration (at a frequency detuning equal to $\pm FSR/2 = 37.5$ MHz) is obtained at a much lower frequency detuning in the double-pass configuration (see the arrows in Fig. 2(b)). Considering that the attenuation of ultrasound waves in biological tissues is proportional to frequency (typically ~0.3 dB/cm/MHz), the double-pass configuration allows obtaining a sufficient rejection of untagged photons without having recourse to high frequency ultrasound, which have a limited penetration depth. The use of a very high finesse single-pass CFPI to obtain the same rejection would reduce the optical etendue of the system (which is inversely proportional to F) and would require mirrors with excessive surface quality. Another approach would be to increase the length of the CFPI to adjust the value of FSR/2 to the ultrasound frequency to get the maximum rejection. For low ultrasound frequencies, this leads to very long CFPI (e.g. 7.5-m long for 5 MHz).

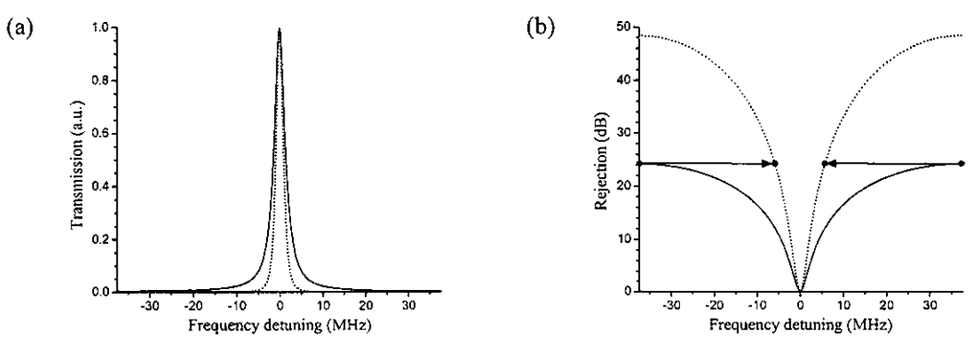

Figure 2 **(a)** Transmission of a 1-m long CFPI (F = 28, FSR = 75 MHz) in single-pass (solid line) and double-pass (dotted line) configuration. **(b)** Rejection of the untagged photons as a function of the frequency detuning of the CFPI in single-pass (solid line) and double-pass (dotted line) configuration.

Most results presented in the literature are obtained with low or moderate power single-frequency continuous-wave (cw) lasers of sufficiently long coherence length [2-7,9]. These sources limit the number of collectable photons at the exit of the scattering medium. For biomedical applications, a direct power scaling is not applicable since the maximum permissible exposure (MPE) in terms of average irradiance is rapidly reached in the visible and the near infrared parts of the spectrum (from 0.2 W/cm^2 to 1.0 W/cm^2). Power scaling is still attractive when considering the low sensitivity of

ultrasound-modulated optical imaging due to a small tagged/untagged photons ratio and to the difficulty of collecting efficiently the photons at the exit of the scattering medium. An appropriate way to apply power scaling is the use of a source emitting a low duty cycle train of powerful laser pulses. Such a laser source can be obtained by amplifying a single-frequency cw laser beam with a flashlamp-pumped gain-switched amplifier. The layout of the master oscillator power amplifier (MOPA) we have used is depicted in Fig. 3(a). Figure 3(b) presents a typical pulse intensity profile at the exit of the MOPA. A peak power of more than 1 kW is routinely attainable with a repetition rate of 25 Hz. The pulse duration was adjustable and typically set to a FWHM of 90 μs to attain the maximum peak power of the MOPA. A 20-μs long part of the pulse (between the dotted line in Fig. 3(b)) was typically used for the measurements. The response of the CFPI being almost instantaneous (a few hundred of nanosecond), the optical illumination of the SM could be limited to the time of flight of the acoustic pulse in the focal zone of the ultrasound beam to reduce the exposure of the sample below the MPE (1 W/cm^2 at 1.064 μm) [11]. Considering that the acoustic focal zone is generally shorter than 30 mm, a pulse duration of approximately 20 μs would be appropriate and could have been obtained form the present MOPA with an electro-optic shutter. Consequently, values of average irradiance mentioned hereafter were calculated by considering laser pulse duration of 20 μs.

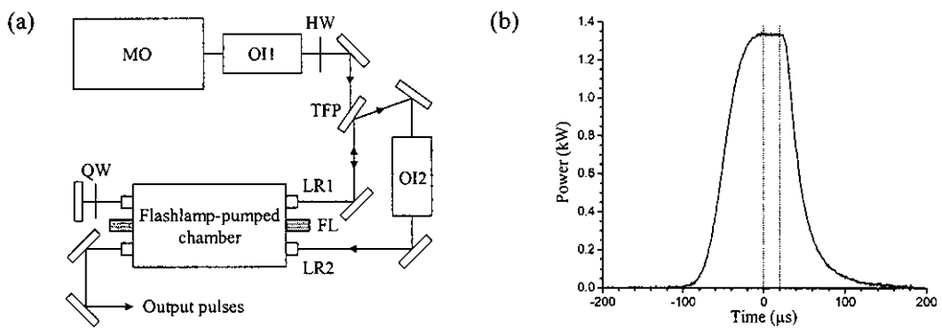

Figure 3 (a) Layout of the Nd:YAG master oscillator power amplifier (MOPA). MO: 200-mW cw master oscillator, OI1-2: optical isolators, LR1-2: Nd:YAG laser rods, FL: flashlamp, HW: half-wave plate, QW: quarter-wave plate, TFP: thin-film polarizer. Other components are plane dielectric mirrors. **(b)** Typical pulse intensity profile at the exit of the MOPA. The useful part of the pulse is enclosed between the dotted lines.

2.2 Characterization of the ultrasonic beam and the scattering medium

The light absorption in water is larger for 1.064 μm wavelength than for wavelength in the therapeutic window. In order to use a scattering medium with an optical absorption coefficient μ_a comparable to that of water in the therapeutic window, we have used a liquid optical phantom based on sunflower oil. The optical absorption of sunflower oil at 1.064 μm was measured to be 3.2×10^{-5} mm^{-1}. As the optical scatterer, we have used titanium dioxide particles (DuPont Ti-PURE R-900, medium particle size: 0.41 μm). In our experiment, the scattering medium was insonified by a 5-MHz focused transducer with an active diameter of 19 mm and a focal length of 45 mm. The transducer was fed with 10-cycle sinusoidal bursts produced by an arbitrary waveform generator and amplified by a high power amplifier. Such a transducer provides a lateral resolution of approximately 0.6 mm in the acoustic focal zone (FWHM of the lateral intensity profile).

The ultrasonic beam was characterized in the transverse plane at the focal distance. The result is shown in Fig. 4(a) in terms of average intensity (during the toneburst) when the UT was fed by the maximum driving voltage. At 5 MHz, the acoustic (intensity) losses coefficient α is equal to 0.37 cm^{-1}. This value is obtained from the expression $16\pi^2\eta f^2/(3\rho c^3)$ where f is the frequency (5 MHz) and the properties of sunflower oil are: the viscosity η = 0.08 Pa·s, the density ρ = 0.92 g/cm^3 and propagation speed of sound c = 1.46 mm/μs [15]. The on-axis pressure was also measured and the axial profile shown in Fig. 4(b) presents, as expected, a local maximum approximately located in the focal plane. The refractive index modulation associated with the propagation of the pressure wave is proportional to the the piezo-optic constant dn/dp of the liquid. The piezo-optic constant (POC) of sunflower oil was measured by using a technique similar to that of Royer *et al.* [16]. We have obtained a POC of 2.5×10^{-10} Pa^{-1}. This value is higher than that of more usual water-based optical phantoms for which the POC is 1.5×10^{-10} Pa^{-1} [17].

In our experiment, we have used an optical phantom composed of titanium dioxide particles dispersed in sunflower oil. The extinction coefficient μ_t of this scattering medium was obtained by the collimated beam transmission method [1]. The scattering mean free path l_s of our phantom was approximately equal to 170 μm at a wavelength of 1.064 μm.

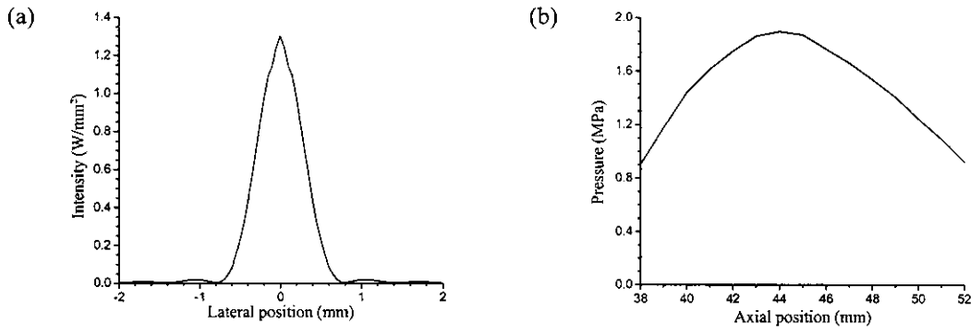

Figure 4 (a) Lateral intensity profile of the acoustic beam in the focal plane of the transducer immersed in sunflower oil. **(b)** Measured on-axis peak-pressure profile.

3. RESULTS

All the measurements were carried out in conditions allowed by the biomedical safety limits [10-11]. The mechanical index (MI) of an ultrasonic wave is given by the ratio $P/\sqrt{f}$ where P is the maximum rarefraction pressure (in MPa) and f is the ultrasound frequency (in MHz). In our experiment, the maximum negative pressure was typically around 1.9 MPa corresponding to MI = 0.85, a value below the safety limit of 1.9. Moreover, at a wavelength of 1.064 μm, the laser beam irradiance must be maintained below a maximum permissible exposure (MPE) of 1.0 W/cm^2. In our experiment, the scattering medium was typically illuminated on a 30-mm diameter surface with 25-mJ pulses (energy in the useful part of the pulse: 20-μs duration and 1.3-kW peak power) at a repetition rate of 25 Hz. Consequently, the average irradiance was approximately equal to 90 mW/cm^2 which is below the MPE by more than a factor 10.

3.1 Properties of the tagged-photon signal

The tagged-photon signal obtained with the double-pass CFPI was first characterized as a function of the ultrasonic excitation of the scattering medium. These signals were obtained with 5-MHz acoustic bursts (10 cycles) in the SM described in section 2.2 (l_s = 170 μm). The thickness of the SM (along the axis y) was equal to 30 mm.

Figure 5 shows the amplitude of the tagged-photon signal as a function of the peak acoustic pressure in the toneburst. The data points correspond to tagged photons shifted by 5 MHz (circles), 10 MHz (triangles), and 15 MHz (squares). A quadratic fit associated with the 5-MHz signals for acoustic pressures below 1 MPa is also shown. As expected, the increase of the tagged-photon signal at 5 MHz is quadratic for lower values of pressure (below 1 MPa). However, it is clearly seen that, at higher acoustic pressures, the second harmonic of the ultrasound frequency is no more negligible and is responsible of the departure of the 5-MHz tagged-photon signal from the quadratic law. Harmonics of the acoustic frequency are attributed to be from optical origin. It appears that the effective modulation depth induced by the pressure wave is sufficiently large to generate multiple optical sidebands.

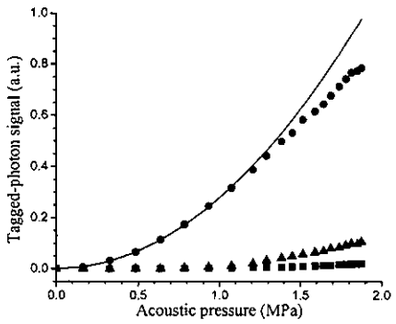

Figure 5 Maximum amplitude of the tagged-photon signal as a function of the acoustic pressure at focus. The data points correspond to tagged photons shifted by 5 MHz (circles), 10 MHz (triangles), and 15 MHz (squares). The curve is a quadratic fit associated with the 5-MHz signals for acoustic pressures below 1 MPa.

3.2 Absorbing object detection in a 30-mm thick scattering medium

In envisioned biomedical applications, the optically absorbing object is often expected to be acoustically matched to the surrounding medium. In our experiment, we have used an optically absorbing cube of polyvinyl alcohol cryogel (PVA-C) which is known to reproduce the acoustic properties of biological tissues [18]. The absorbing cube was suspended at a fixed position in the liquid scattering medium with a 65-μm diameter copper wire.

B-scan images were obtained by moving the transducer along the axis x (the orientation of the axes is given in Fig. 1), all other components of the setup being fixed. The lateral step of the transducer was 0.25 mm. Each vertical line (A-scan) of the image is obtained by the temporal to spatial mapping related by the acoustic propagation speed ($c \sim 1.5$ mm/μs). The temporal sampling rate was equal to 5 MS/s which corresponds to one (vertical) pixel per 0.30 mm. The B-scan image is then obtained by a juxtaposition of A-scan with a lateral step (parallel to the axis x) equal to the lateral step of the transducer i.e. one (horizontal) pixel per 0.25 mm.

Figure 6 shows the results obtained with the scattering medium (l_s = 170 μm) described in section 2.2 enclosed in a 30-mm thick plexiglas cell. The transverse dimensions of the cell were 60 mm along the axis x and 90 mm along the axis z. The laser beam and the COF were both centered at ~45 mm below the transducer. The scattering medium was insonified with 5-MHz tonebursts (10 cycles). Both images were obtained with a 3x3x3-mm^3 optically absorbing and acoustically transparent cube of PVA-C located in the focal plane of the transducer. A local decrease of the tagged-photon signal level is clearly observed. The vertical A-scan profile and the horizontal intensity profile passing through the center of the dark region are also shown for each image. The image on the left was obtained without averaging (single pulse per vertical line) while the image on right was obtained by averaging 16 A-scan for each vertical line. The SNR is clearly acceptable without averaging. In both images, the limited lateral extent of the tagged photons captured by the COF is seen by the surrounding dark region.

The horizontal extent along the x-axis of the drop of the tagged-photon signal is expected to be equal to the convolution of the transverse acoustic beam profile shown Fig. 4(a) and the spatial extent of the absorbing object along the x-axis (3 mm).

The vertical extent along the z-axis of the drop of the tagged-photon signal is expected to be equal to the convolution of the 3-mm spatial extent of the toneburst along the ultrasound axis (10 cycles of 0.3 mm) with the dimension of the absorbing object in the same direction which is also 3 mm in this case.

The good acoustic transparency of PVA-C is confirmed in Fig. 6 by the presence of tagged photons below the absorbing object. For the sake of comparison, Fig. 7 shows a result obtained with an optically absorbing object which is also acoustically absorbing. In this case a small sphere of black modeling compound was suspended in the SM. The acoustic shadow is clearly seen below the central dark region.

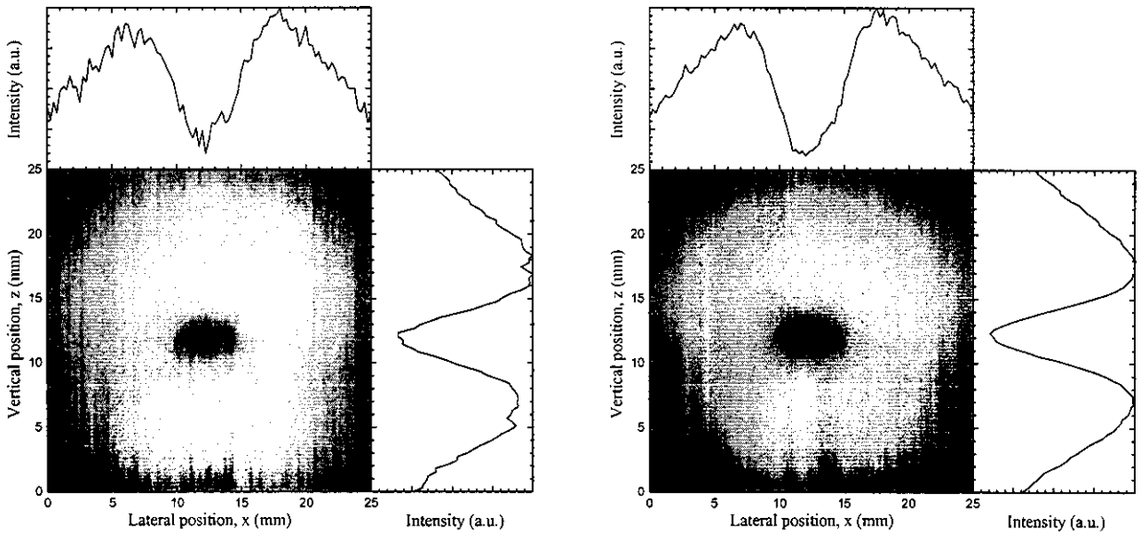

Figure 6 B-scan images obtained in a 30-mm thick scattering medium containing an optically absorbing cube (3x3x3 mm^3) of PVA-C (which is acoustically transparent) by using 5-MHz acoustic bursts (10 cycles). The vertical A-scan profile (curves on right) and the horizontal profile (upper curves) passing through the optically absorbing object are also shown. The image on left was obtained with a single laser pulse per A-scan and the image on right was obtained by averaging 16 pulses per A-scan.

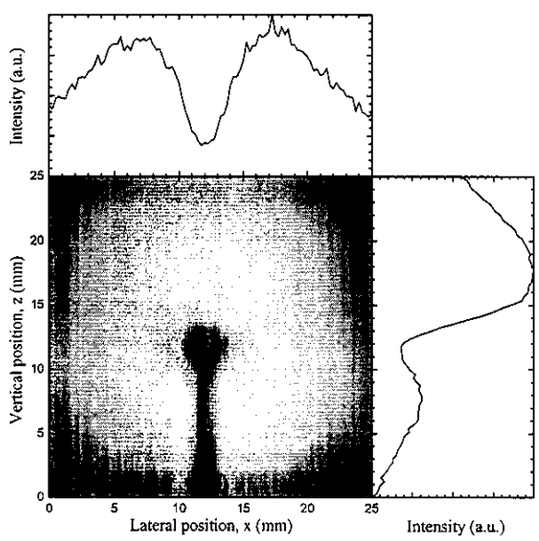

Figure 7 B-scan image obtained in a 30-mm thick scattering medium containing an optically and acoustically absorbing sphere of black modeling compound. The medium was insonified with 5-MHz acoustic bursts (10 cycles). The vertical A-scan profile (curve on right) and the horizontal profile (upper curve) passing through the absorbing object are also shown.

3.3 Tagged-photon signals in a 60-mm thick scattering medium

Measurements described in section 3.2 were obtained with a single laser pulse by using a short 5-MHz acoustic burst (10 cycles) in a 30-mm thick scattering medium. In this section, we describe a measurement performed using the same scattering medium enclosed in a 60-mm thick plexiglas cell. Again, the scattering medium was insonified with 5-MHz tonebursts (10 cycles) and a 3x3x3-mm^3 optically absorbing and acoustically transparent cube was located in the focal plane of the transducer. The resulting image is shown in Fig. 8. In this case, each A-scan was obtained by averaging 256 tagged-photon signals. When comparing the image in Fig. 8 with those of Figs. 6 and 7, it is clear that the lateral extent of the tagged-photon signal is much broader, as expected in a thicker SM.

In the present version of the setup, the SNR is limited by the technical noise of the InGaAs-PIN photodiode. However, as mentioned earlier, the peak power could be made 10 times higher without exceeding the MPE at 1.064 μm. Moreover, the acoustic amplitude could also be raised. Consequently, even in a 60-mm thick SM, an acceptable SNR could be obtained by using a single pulse per A-scan. The SNR could also be further enhanced by using an avalanche photodiode with an appropriate internal gain. These enhancements in terms of SNR could also be used to increase the spatial resolution of the technique and/or the depth of the probed region.

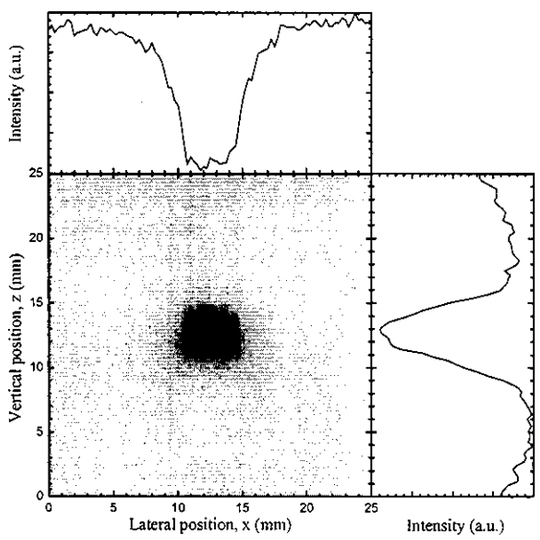

Figure 8 B-scan image obtained in a 60-mm thick scattering medium containing an optically absorbing (and acoustically transparent) cube of 3x3x3 mm^3. The medium was insonified with 5-MHz acoustic bursts (10 cycles). The vertical A-scan profile (curve on right) and the horizontal profile (upper curve) passing through the absorbing object are also shown.

4. CONCLUSIONS

Although the optical etendue of the CFPI is low when compared to other detection schemes, the rejection of the untagged photons in a double-pass configuration is sufficiently high to detect selectively the tagged photons. In this work, the low etendue has been compensated by a high power laser source. A low duty cycle pulse train with high peak power concentrates the illumination of the scattering medium during the transit time of the acoustic pulse while maintaining the average power below the maximum permissible exposure.

The spatial resolution along the ultrasound axis was obtained by using few-cycle acoustic bursts and the lateral resolution was obtained by using a focused ultrasound beam. Tagged-photon signals were obtained in a truly scattering propagation regime without going beyond the biomedical safety limits in terms of ultrasonic wave amplitude and laser beam irradiance. The detection of an optically absorbing object in a 30-mm thick scattering medium was performed

without averaging with 10-cycles acoustic bursts at 5 MHz. By allowing averaging with 256 pulses, an absorbing object of 3x3x3 mm^3 was detected inside a 60-mm thick scattering medium. The use of an acoustic wave with the maximum amplitude allowed by safety limits and a laser beam with the maximum permissible exposure and optimum duration would have been sufficient to obtain single-shot measurements with the same signal-to-noise ratio.

The results presented here demonstrate the pertinence of a high power laser source to allow the detection of optically absorbing objects in very thick scattering media by using ultrasound-modulated optical imaging. The optical etendue and the rejection of the untagged photons could be both enhanced by using a longer (folded) double-pass CFPI.

ACKNOWLEDGEMENTS

The authors would like to thank Gordon Campbell for providing samples of PVA-C.

REFERENCES

1. L. V. Wang, H. Wu, *Biomedical Optics: Principles and Imaging*, John Wiley and Sons, Inc., Hoboken, New Jersey, 2007.
2. L. Wang, S. L. Jacques, and X. Zhao, "Continuous-wave ultrasonic modulation of scattered laser light to image objects in turbid media," Opt. Lett. **20**, 629-631 (1995).
3. S. Sakadzic and L. V. Wang, "High-resolution ultrasound-modulated optical tomography in biological tissues," Opt. Lett. **29**, 2770-2772 (2004).
4. S. Lévêque, A. C. Boccara, M. Lebec, and H. Saint-Jalmes, "Ultrasonic tagging of photon paths in scattering media: parallel speckle modulation processing," Opt. Lett. **24**, 181-183 (1999).
5. M. Atlan, B. C. Forget, F. Ramaz, A. C. Boccara, and M. Gross, "Pulsed acousto-optic imaging in dynamic scattering media with heterodyne parallel speckle detection," Opt. Lett. **30**, 1360-1362 (2005).
6. T. W. Murray, L. Sui, G. Maguluri, R. A. Roy, A. Nieva, F. Blonigen, and Ch. A. DiMarzio, "Detection of ultrasound-modulated photons in diffuse media using the photorefractive effect," Opt. Lett. **29**, 2509-2511, (2004).
7. F. Ramaz, B. C. Forget, M. Atlan, A. C. Boccara, M. Gross, P. Delaye, and G. Roosen, "Photorefractive detection of tagged photons in ultrasound modulated optical tomography of thick biological tissues," Opt. Express **12**, 5469-5474 (2004).
8. G. Rousseau, A. Blouin, and J.-P. Monchalin, "Ultrasound-modulated optical imaging using a powerful long pulse laser," Opt. Express **16**, 12577-12590 (2008).
9. Youzhi Li, Huiliang Zhang, Kim Chulhong, K. H. Wagner, P. Hemmer, and L. V. Wang, "Pulsed ultrasound-modulated optical tomography using spectral hole burning as a narrowband spectral filter," Appl. Phys. Lett. **93**, 011111 (2008).
10. F. A. Duck, "Medical and non-medical protection standards for ultrasound and infrasound," Prog. biophys. molec. biol. **93**, 176-191 (2007).
11. Laser Institute of America, *American national standard for safe use of lasers* (ANSI Z136.1-2000), ANSI, Orlando, Florida, 2000.
12. M. Hercher, "The spherical mirror Fabry-Perot interferometer," Appl. Opt. **7**, 951-963 (1968).
13. J. R. Sandercock, "Brillouin scattering study of SbSI using a double-passed, stabilised scanning interferometer," Opt. Commun. **2**, 73–76 (1970).
14. D. S. Cannell, J. H. Lunaceck, and S. B. Dubin, "A simple double-pass spherical Fabry-Perot interferometer," Rev. Sci. Instrum. **44**, 1651–1653 (1973).
15. L. E. Kinsler and A. R. Frey, *Fundamentals of Acoustics*, John Wiley and Sons, Inc., New York, 1962.
16. D. Royer, N. Dubois, and M. Fink, "Optical probing of pulsed, focused ultrasonic fields using a heterodyne interferometer," Appl. Phys. Lett. **61**, 153-155 (1992).
17. W. A. Riley and W. R. Klein, "Piezo-optic coefficients of liquids," J. Acous. Soc. Am. **42**, 1258-1261 (1967).
18. K. J. M. Surry, H. J. B. Austin, A. Fenster, and T. M. Peters, "Poly(vinyl alcohol) cryogel phantoms for use in ultrasound and MR imaging," Phys. Med. Biol. **49**, 5529–5546 (2004).